Optimization of a cardiac tissue segmentation pipeline in murine whole-heart reconstructions

F. Giardini*[1,2], E. Barcali*[2,3], M. De Santis[2], B. Olmi[2], E. Lazzeri[1], C. Nardi[3] and L. Bocchi[2]
[1]*European Laboratory for Non-Linear Spectroscopy (L.E.N.S.), Sesto Fiorentino, Italy*
[2]*Dept. of Information Engineering, University of Florence, v. Santa Marta, 3 - Florence, Italy*
[3]*Dept. of Biomedical Experimental and Clinical Sciences "Mario Serio", University of Florence, Florence, Italy*

***Abstract*—Image segmentation is an important branch of modern image processing, especially in biomedical or microscopy image analysis. Novel optical imaging techniques such as Light-Sheet Fluorescent Microscopy (LSFM) allow the reconstruction of massive biological samples with micron-scale spatial resolution. In this context, image segmentation is challenging due to the high variability of LSFM images. This article describes the optimization of an automatic segmentation pipeline to identify the cardiac tissue in LSFM-based high-resolution 3D reconstructions of five murine hearts, previously cleared and stained with Wheat Germ Agglutinin (WGA). We address the challenge using Trainable WEKA (Waikato Environment for Knowledge Analysis) Segmentation, a plug-in of Fiji software. Three different training sets were generated by means of a manual ground truth combined with two additional feature selection algorithms included in WEKA: CorrelationAttributeEvaluator and InfoGainAttributeEvaluator. To speed up the computational time, we also defined a reduced training dataset selecting only common features between the two sets: median diffusion, mean, anisotropy, and entropy. We trained four different classifiers for each of the three training sets in order to identify myocardium tissue from the background: RandomForest, J48, NaiveBayes, and MultilayerPerceptron. The performance of the classifiers was evaluated for each training set and we found that the RandomForest is the more accurate and stable model over different datasets with a Dice similarity coefficient of 0.895, 0.895, and 0.892, respectively. Results highlight the reliability of RandomForest to address high-resolution image segmentation, allowing the generation of 3D whole-heart reconstruction useful to investigate, in the future, structural features in pathological mouse models.**

***Keywords*—Trainable Weka Segmentation, Fiji, light-sheet fluorescence microscopy, cardiac tissue**

I. Introduction

The World Health Organization (WHO) estimates that 17.9 million people worldwide die of cardiovascular disease (CVD) every year [1]. Research in recent years has made many advances in this field to improve diagnosis, treat these diseases better, and reduce CVD mortality [2].

Several imaging modalities can be applied to studying the heart, including echography, CT, coronary angiography, PET, and MRI [3], [4]. All of these techniques are characterized by insufficient spatial resolution and the inability to detect fluorescence-marked particles usually used in biomedical research [5], [6], [7]. On the other hand, due to the intrinsic opacity of the cardiac tissue, conventional microscopy techniques have the disadvantage of requiring the use of small working distances, or a mechanical slicing of the sample, thus introducing the consequent risks of modifying sample dimensions, preventing a reliable three-dimensional (3D) reconstruction. Light Sheet Fluorescence Microscopy (LSFM), combined with novel advanced tissue-clearing techniques, overcomes these limitations [8], [9].

LSFM consists in illuminating the transparent sample with a single thin sheet of light orthogonally oriented to the detection path so that only the excited optical plane of the tissue is detected. The sample is then moved in an axial direction to perform a tomographic scan, imaging the volume section-by-section, and thus creating a 3D model after a post-processing step [10], [11], improving image contrast and allowing high speed and precise monitoring of cells or tissues combined with fluorescent multi-labeling within a complex and dynamic environment such as the cardiovascular one [12], [13]. LSFM image segmentation lacks fully automated techniques because of the inherent variability of images obtained with this imaging technique. New deep-learning techniques are emerging and showing good results, but currently manual segmentation remains the gold standard in terms of reliability. Naturally, automatic classification overcomes the problems associated with manual segmentation, which is time-consuming and sensitive to high inter- and intra-operator variability [3].

In this study, we optimized a system capable of automatically segmenting cardiac tissue in LSFM reconstructions of cleared adult murine hearts. To this aim, we adopted a plug-in from Fiji, Trainable Weka Segmentation (TWS), to perform a two-step optimization: first, we identified the most significant features to discriminate the tissue from the background with two different algorithms; then, we trained four models on the different training datasets to perform a real segmentation, finally comparing their performance. The ultimate goal of our project is to generate a 3D model of the heart anatomy, thus correlating, in the future, structural features between heart remodeling and electrical heart dysfunctions in pathological murine models.

II. Material And Methods

The present investigation is applied to five three-dimensional reconstructions of cleared hearts of control mice of 6 months (C57BL/6J). The experimental protocol was approved by the Italian Ministry of Health (protocol number 647/2015-106 PR). All the animals were provided by ENVIGO, Italy. Samples reconstructions were obtained by

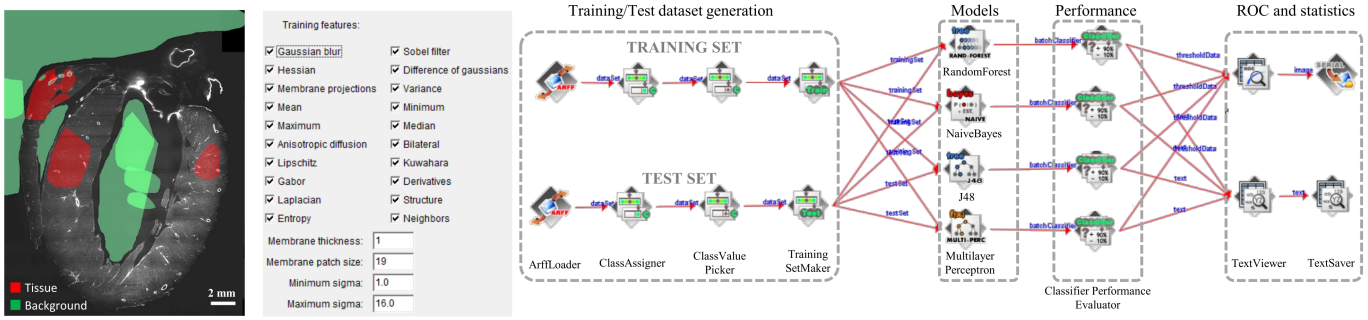

(a) (b) (c)

Fig. 1: a) Representative longitudinal view of a cleared mouse heart reconstruction generated with light-sheet microscopy by staining cellular membranes (pixel size: 20.8 µm). A manual classification of *tissue* (red) and *background* (green) is superimposed on the image as an example of ground truth. b) Features selected to generate the training test using the Trainable Weka Segmentation (TWS) plugin. c) Scheme of the training/test workflow implemented using the tool *KnowledgeFlow* included in TWS. The main parts are highlighted with dashed gray lines.

performing a three-step imaging protocol: tissue clarification with CLARITY method optimized for the cardiac tissue [14], [15]; staining of cellular membranes with Wheat Germ Agglutinin (WGA) conjugated with Alexa Fluor 633; imaging by tiles with a custom-made light-sheet microscope [16] with an original voxel size of $0.65\,\mu m \times 0.65\,\mu m \times 2\,\mu m$ in x, y and z axis respectively. Final reconstruction was obtained by stitching tiles with custom-made software [17]. In this paper, three-dimensional (3D) images are downsampled to an isotropic pixel size of $20.8\,\mu m$.

Cardiac tissue segmentation is performed frame-by-frame in two-dimension (2D) using the plugin TWS, included in the image analysis software Fiji [18], [19], evaluating different classification models on three different sets of features.

A. Preliminary dataset and ground-truth

The preliminary dataset used to identify key features for prediction consists of ten images at different depths from the reconstruction of a single control mouse heart. By starting the TWS plugin, the two classes of interest "Tissue" and "Background" were defined. Ground truth was generated by manually classifying different regions of interest (ROIs) (Figure 1a) in all 10 frames. In the "Settings" tab, all features offered by the WEKA software were selected (Figure 1b) to generate as many features as possible from the images. Next, dimensionality reduction was performed using two different selection algorithms.

B. Feature extraction

Dimensionality reduction was performed using the "Select Attributes" tool in Weka Explorer. This is based on the joint action of an attribute evaluation algorithm (Attribute Evaluator) and a search algorithm (Search Method). The first evaluates each attribute in the data set in relation to the desired classification; the latter determines the most meaningful combination of attributes for the classification. Among the algorithms for attribute selection supported by Weka, we selected:

- CorrelationAttributeEvaluator: calculates the correlation between each attribute and the output variable: attributes are the more significant the closer the correlation values are to 1.
- InfoGainAttributeEvaluator: calculates the entropy of each attribute in relation to the output variable: attributes are the more significant the closer the entropy values are to 1.

In the present study, both evaluation algorithms described above were used, generating two different sets of features (defined as *Correlation set* and *InfoGain set* for simplicity). A set of the common attributes between the previous two sets was also considered and defined as *reduced set*.

C. Classifiers

The tool *KnowledgeFlow* presents a "data-flow"-inspired interface for Weka. Users can select Weka components from a toolbar, place them on a layout canvas, and link them together to form a "knowledge flow" for data processing and analysis. Here, the following classifiers were tested:

- RandomForest: this is the default algorithm when implementing a classifier in Weka;
- J48: characterized by a fast learning process;
- NaiveBayes: the Bayesian classifier is generally reliable and compact;
- MultilayerPerceptron: a classifier widely used in imaging, based on a supervised learning technique called *back-propagation*.

To compare these classifiers, we generate the KnowledgeFlow shown in Figure 1c.

D. Training set and test set

The training and the test datasets were generated by first selecting randomly 40 and 30 images from the five different reconstructions, respectively, and then manually labeling tissue and background on these images. Then we extracted from labeled images the three different sets of features derived through Weka Explorer: Correlation set, InfoGain set, and reduced set, thus generating three versions of training and test datasets. Exploiting the workflow shown in Figure 1c, the four

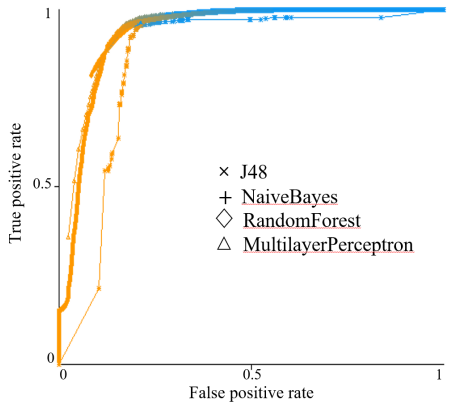

Fig. 2: ROC curve of the four models tested on the *reduced set* of features.

TABLE I: Dice similarity coefficient

Classifier	Correlation set	InfoGain set	Reduced set
J48	0.869	0.889	0.879
NaiveBayes	0.881	0.880	0.888
RandomForest	0.895	0.895	0.892
MultilayerPerceptron	0.872	0.893	0.865

different models were trained on the same training set and then used to classify the test set. Finally, the performance of each model was assessed by the "ClassifierPerformanceEvaluator" module, generating numerical statistics and plotting the Receiver operating characteristic (ROC) curve.

III. Results

Feature selection was performed using two different algorithms: the CorrelationAttributeEvaluator and the InfoGainAttributeEvaluator. In both cases, we defined the selection threshold as the correlation value obtained using the original image as a feature, without extracting any statistical index or morphological operator. In the first case, the correlation of the original image was 0.474554. The following features, having a correlation value larger than 0.474554, were selected: median, mean, anisotropic diffusion, entropy, membrane projection, Gaussian blur, and minimum. These were defined as *Correlation set*. With the second approach, the correlation of the original image was 0.53931, and the algorithm then identifies as fundamental those features with a correlation value larger than 0.53931, namely: median, mean, anisotropic diffusion, entropy, variance, and maximum, that were defined as *InfoGain set*. We defined also a *reduced set* of features, composed of the subset of features in common with the previous two sets: median, mean, anisotropic diffusion, and entropy.

The four models were trained and tested using these three different sets of features. The Dice similarity coefficient values for the 4 models and for the three different feature sets (Correlation, InfoGain, and reduced sets respectively) are shown in Table I.

The model with the best performance is the RandomForest for all the feature sets, and the error of this model is less variable than the other models over the different feature sets. Using the reduced set of features, the ROC curve of the four models is generated and shown in Figure 2, and the main metrics of the selected model (RandomForest) are reported in Table II.

TABLE II: RandomForest Performance

Class	TP Rate	FP Rate	Precision	Recall	F-Measure	ROC Area
Tissue	0.975	0.211	0.837	0.975	0.901	0.940
Background	0.789	0.025	0.966	0.789	0.869	0.940
Weighted Avg.	0.887	0.123	0.898	0.887	0.886	0.940

Finally, a tissue segmentation was performed on an entire mouse heart reconstruction (Figure 3a shows a representative frame of the sample classified). The 3D image was segmented frame-by-frame using the RandomForest trained with the reduced set of features. This model assigns to each pixel a probability $\mathbf{p} \in [0, 1]$ of belonging to the "tissue" class (Figure 3b). The final binary segmentation can be obtained by applying an arbitrary threshold on that probability map (here, the threshold is set $p = 0.5$, Figure 3c). A 3D segmentation is shown in Figure 3d. The model was able to correctly segment the myocardial tissue also in the regions affected by a low fluorescence signal intensity, without being affected by the variability of the background brightness.

IV. Discussion and Conclusion

This work aimed to optimize a software pipeline for cardiac tissue segmentation in LSFM reconstructions of cleared whole murine hearts. This aspect is important for the investigation of cardiac functioning [20], allowing in the future to correlate structural cardiac tissue remodeling with electrical dysfunctions of the heart detected by novel optical mapping techniques in murine hearts [21], [22]. The work was articulated in three phases: first, we manually segmented the cardiac tissue from the background frame-by-frame in 2D with a plugin of Fiji, TWS, then we extrapolated the most significant attributes exploiting two different feature selection algorithms included in WEKA and finally, we tested different models to evaluate their accuracy on two different ROIs: tissue and background. The optimized pipeline applied to the 3D reconstruction of the hearts showed a good functioning of our system providing a good approach for automatic segmentation of LSFM images. It could be interesting to perform the same test with more powerful processors, using a larger dataset. The main limit was connected to the resolution of the images and the reduced dataset. An improvement of the work could be to use a larger data set and involve images with a higher spatial resolution. The proposed method, applied to reconstructions of hearts of control and pathological models, will allow the extraction of anatomical features, enabling the quantification of the structural remodeling occurring in pathological hearts.

References

[1] World Health Organization, Cardiovascular diseases (CVDs), 2021, June 1, retrieved from https://www.who.int/en/news-room/fact-sheets/detail/cardiovascular-diseases-(cvds)

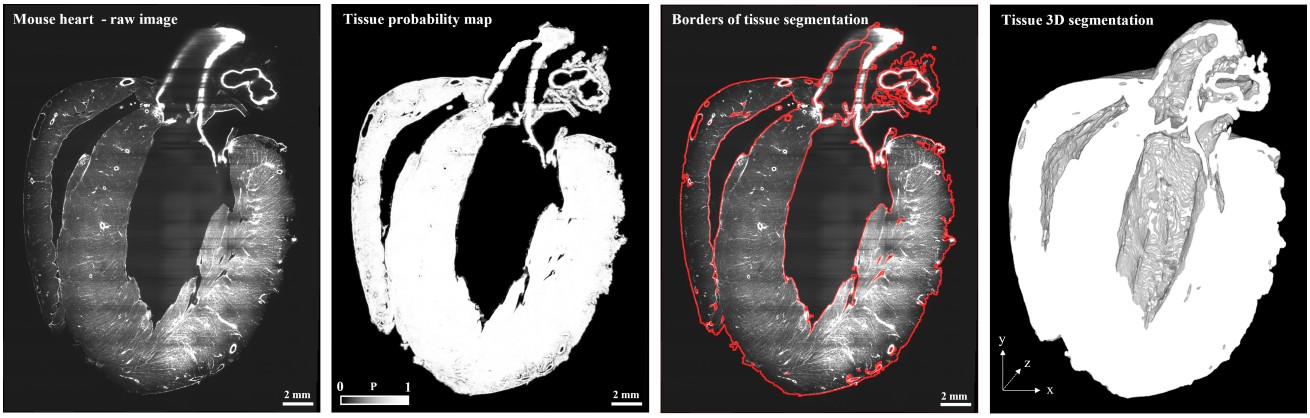

(a) (b) (c) (d)

Fig. 3: a) Representative frame of a cleared murine heart stained with WGA and reconstructed with light-sheet microscopy. b) Classification of the image in (a) obtained with the RandomForest trained on the *reduced* features set. The intensity of each pixel (from 0 to 255) is proportional to the probability (from 0, *background*, to 1, *tissue*) of falling into the "tissue" class. c) The borders (red lines) of the binary segmentation obtained by thresholding the probability map shown in (b) with a value of $p = 0\,5$ are superimposed on the original frame shown in (a). d) Longitudinal view of the three-dimensional reconstruction of the heart anatomy obtained by rendering 2D tissue segmentation at different depths.

[2] C. Chen, C. Qin, H. Qiu, G. Tarroni, J. Duan, W. Bai, D. Rueckert, Deep Learning for Cardiac Image Segmentation: A Review, Frontiers in cardiovascular medicine, vol. 7, no. 25, 2020, https://doi.org/10.3389/fcvm.2020.00025.

[3] C. Petitjean, J.N. Dacher, Dacher, J.: A review of segmentation methods in short axis cardiac MR images, Medical Image Analysis, vol. 15, pp. 169-184, 2011, 10.1016/j.media.2010.12.004.

[4] Y. Ding, J. Lee, J.J. Hsu, C.C. Chang, K.I. Baek, S. Ranjbarvaziri, R. Ardehali, R.R.S. Packard, T.K. Hsiai, Light-Sheet Imaging to Elucidate Cardiovascular Injury and Repair, Curr. Cardiol. Rep., vol. 20, no. 5, pp.35, 2018, doi: 10.1007/s11886-018-0979-6.

[5] A.J. Kim, R. Francis, X. Liu, W.A. Devine, R. Ramirez, S.J. Anderton, L.Y. Wong, F. Faruque, G.C. Gabriel, W.Chung, L. Leatherbury, K. Tobita, C.W. Lo, Microcomputed tomography provides high accuracy congenital heart disease diagnosis in neonatal and fetal mice, Circ Cardiovasc Imaging, vol.6, no. 4. pp. 551-9, 2013, doi: 10.1161/CIRCIMAGING.113.000279. Epub 2013 Jun 12. Erratum in: Circ Cardiovasc Imaging. 2013 Sep;6(5):e30. Chung, Wendy [added]. PMID: 23759365; PMCID: PMC3908688.

[6] C. Baltes, N. Radzwill, S. Bosshard, D. Marek, M. Rudin, Micro MRI of the mouse brain using a novel 400 MHz cryogenic quadrature RF probe, NMR Biomed. vol. 22, no. 8, pp. 834-42, 2009 Oct, doi: 10.1002/nbm.1396.

[7] C. Olianti, I. Costantini, F. Giardini, E. Lazzeri, C. Crocini, C. Ferrantini, F.S. Pavone, P.G. Camici, L. Sacconi, 3D imaging and morphometry of the heart capillary system in spontaneously hypertensive rats and normotensive controls, Sci Rep. vol. 10, no. 1, pp. 14276, 2020, https://doi.org/10.1038/s41598-020-71174-9

[8] Y. Ding, J. Lee, J. Ma, K. Sung, T. Yokota, N. Singh et al., Light-sheet fluorescence imaging to localize cardiac lineage and protein distribution, Sci Rep, vol. 7, no. 42209, 2017, https://doi.org/10.1038/srep42209

[9] C. Olianti, F. Giardini, E. Lazzeri, I. Costantini, L. Silvestri, R. Coppini, E. Cerbai, F. S. Pavone, L. Sacconi, et al., Optical clearing in cardiac imaging: A comparative study, Prog. Biophys. Mol., vol. 168, pp. 10-17, 2022, https://doi.org/10.1016/j.pbiomolbio.2021.07.012.

[10] Y. Ding, Z. Bailey, V. Messerschmidt, J. Nie, R. Bryant, S. Rugonyi, P. Fei, J. Lee, T.K. Hsiai, Light-sheet Fluorescence Microscopy for the Study of the Murine Heart, J Vis Exp, vol. 15; no. 139, pp. 57769, https://doi.org/10.3791/57769

[11] P.A. Santi, Light sheet fluorescence microscopy: a review, J Histochem Cytochem, vol. 59, no.2, pp.129-38, 2011, doi: 10.1369/0022155410394857.

[12] P. Fei, J. Lee, R. Packard, K.-I. Sereti, H. Xu, et al. Cardiac Light-Sheet Fluorescent Microscopy for Multi-Scale and Rapid Imaging of Architecture and Function. Sci Rep, vol. 6, no. 22489, 2016, https://doi.org/10.1038/srep22489

[13] Z. Wang, Y. Ding,S. Satta, M. Roustaei, P. Fei et al. A hybrid of light-field and light-sheet imaging to study myocardial function and intracardiac blood flow during zebrafish development, PLOS Computational Biology, vol. 17, no. 7, pp. e1009175, 2021. https://doi.org/10.1371/journal.pcbi.1009175

[14] K.Chung, J. Wallace, S.Y. Kim, S. Kalyanasundaram, A. S. Andalman ET AL. Structural and molecular interrogation of intact biological systems. Nature, vol. 497, pp. 332–337 2013. https://doi.org/10.1038/n.

[15] F. Giardini, E. Lazzeri, C. Olianti, G. Beconi, I. Costantini, L. Silvestri, E. Cerbai, F.S. Pavone, L. Sacconi, Mesoscopic Optical Imaging of Whole Mouse Heart. J. Vis. Exp. vol. 176, pp. e62795, 2021, doi:10.3791/62795

[16] L. Silvestri, M.C. Müllenbroich, I. Costantini, A. P. Di Giovanna, G. Mazzamuto, A. Franceschini, Universal autofocus for quantitative volumetric microscopy of whole mouse brains. Nat Methods vol. 18, pp. 953–958, 2021, https://doi.org/10.1038/s41592-021-01208-1.

[17] G. Mazzamuto, "ZetaStitcher: a software tool for high-resolution volumetric stitching,", https://github.com/lens-biophotonics/ZetaStitcher.

[18] J. Schindelin, I. Arganda-Carreras, E. Frise, V. Kaynig, M. Longair et al. Fiji: an open-source platform for biological-image analysis. Nature Methods, vol. 9, no. 7, pp. 676–682, 2012, doi:10.1038/nmeth.2019

[19] I.H. Witten, E. Frank . Data Mining: Practical Machine Learning Tools and Techniques, 2nd edition. Morgan Kaufmann, San Francisco, 2005.

[20] T. Seidel, T. Draebing, G. Seemann, F.B. Sachse . A Semi-automatic Approach for Segmentation of Three-Dimensional Microscopic Image Stacks of Cardiac Tissue. Lecture Notes in Computer Science, vol 7945. Springer, Berlin, Heidelberg., 2013 https://doi.org/10.1007/978-3-642-38899-6_36

[21] F. Giardini, V. Biasci, M. Scardigli, F.S. Pavone, G. Bub, and L. Sacconi, A Software Architecture to Mimic a Ventricular Tachycardia in Intact Murine Hearts by Means of an All-Optical Platform. Methods Protoc. 2019, 2, 7. https://doi.org/10.3390/mps2010007

[22] Biasci, V., Santini, L., Marchal, G.A. et al. Optogenetic manipulation of cardiac electrical dynamics using sub-threshold illumination: dissecting the role of cardiac alternans in terminating rapid rhythms. Basic Res Cardiol 117, 25 (2022). https://doi.org/10.1007/s00395-022-00933-8